Received: 10 September 2025 | Revised: 20 April 2026 | Accepted: 10 June 2026 | Published online: 23 July 2026

RESEARCH ARTICLE

Journal of Computational and Cognitive Engineering
2026, Vol. 00(00) 1–15
DOI: 10.47852/bonviewJCCE62027633

BON VIEW PUBLISHING

Enhanced Rotating Machinery Fault Diagnosis Using Holo-Hilbert Spectrum Analysis and Machine Learning

Van-Trung Nguyen[1,*], Ba-Tan Le[1] and Van-Phuong Dao[2]

[1] *Department of Renewable Energy, Ho Chi Minh City University of Technology and Education, Vietnam*

[2] *Faculty of Electrical and Electronics Engineering, Ho Chi Minh City University of Technology and Education, Vietnam*

Abstract: Reliable fault diagnosis in rotating machinery is challenging due to the nonlinear and non-stationary nature of vibration signals. Although time–frequency analysis is widely used, it cannot capture the cross-scale coupling between amplitude-modulated (AM) and frequency-modulated (FM) components that carry essential diagnostic information. This study applies Holo-Hilbert Spectrum Analysis (HHSA) to extract amplitude–frequency modulation features and integrates them with six machine learning classifiers to identify four fault conditions. Random Forest, K-Nearest Neighbors, and Logistic Regression achieve accuracies of up to 99.95%, yielding higher accuracy than Fast Fourier Transform-based features. The proposed framework employs an HHSA-based feature extraction pipeline that effectively captures AM–FM coupling in nonlinear vibration signals. It also provides higher discriminative capability than traditional spectral approaches and maintains robustness across multiple classifiers. This method offers high diagnostic accuracy and strong potential for industrial predictive maintenance. Future work will focus on improving computational efficiency and evaluating the framework under more diverse and realistic operating conditions.

Keywords: rotating machinery, fault diagnosis, Holo-Hilbert Spectrum Analysis, machine learning, feature extraction

1. Introduction

Rotating machinery, including bearings, gears, motors, turbines, and shafts, is an essential element in many industries, encompassing manufacturing, transportation, energy, aerospace, wind power, and automotive systems [1, 2]. These machines are indispensable for the transformation of energy into mechanical motion, as they facilitate the effective functioning of production lines, vehicles, and power generation facilities. Given their critical role, unexpected failures may result in significant consequences, such as costly operational delays, safety hazards, and considerable damage to equipment. For example, a bearing failure in a high-speed turbine may halt power production and cause extensive operational disruptions. For this reason, reliable operation requires effective fault diagnosis capable of identifying early-stage degradation before it evolves into critical failure.

Early detection facilitates prompt maintenance actions, thereby minimizing expenses, improving equipment uptime, extending component lifespan, and enhancing industrial safety. The growing implementation of smart manufacturing and condition-based monitoring underscores the significance of precise fault diagnosis within contemporary predictive maintenance frameworks, as it underpins data-informed decision-making and mitigates dependence on predetermined maintenance schedules.

Consequently, fault diagnosis and predictive maintenance have emerged as essential methodologies for assessing machinery health, preventing operational failures, and refining maintenance planning. These approaches are congruent with the tenets of Industry 4.0 and smart manufacturing, capitalizing on data-driven methodologies to improve operational effectiveness and reduce unplanned downtime [3]. Fault diagnosis typically involves the detection, identification, and localization of faults based on physical signal measurements [4], while predictive maintenance extends this by forecasting the remaining useful life and enabling condition-based maintenance actions that reduce costs and improve reliability [5]. However, accurate fault diagnosis is still difficult, particularly due to the nonlinear and non-stationary nature of vibration signals from rotating machinery. These signals are affected by changes in operating speed, loads, and environmental conditions, and they typically contain complex interactions between impulsive components, harmonics, sidebands, and transient features that change over time [6–8]. Traditional fault diagnosis methods, which assume linearity and stationarity, struggle to capture these dynamic characteristics, often leading to misdiagnosis or missed faults.

To address these challenges, many signal processing algorithms have been proposed, each designed to extract distinct attributes from vibration signals. The Fast Fourier Transform

*Corresponding author: Van-Trung Nguyen, Department of Renewable Energy, Ho Chi Minh City University of Technology and Education, Vietnam. Email: trungnv@hcmute.edu.vn

(FFT) is frequently utilized to examine vibration signals within the frequency domain, allowing the detection of characteristic frequencies related to mechanical faults [6]. Nevertheless, the FFT's inherent assumption of signal stationarity constrains its utility when analyzing transient and time-varying fault characteristics that are typical of actual operational environments [7]. Wavelet transform (WT) methodologies offer an enhancement by enabling joint time–frequency analysis (TFA), thereby improving the detection of transient occurrences and non-stationary features within vibration signals [9]. Envelope analysis is another technique commonly used for bearing fault diagnosis, focusing on demodulating high-frequency resonance to reveal low-frequency fault impacts. Nonetheless, these methods depend on the appropriate selection of wavelets or filters and require high signal-to-noise ratios, which are frequently challenging to ensure in industrial settings [10].

Adaptive data-driven methodologies, including Empirical Mode Decomposition (EMD) and Hilbert-Huang Transform (HHT), have gained attention for their ability to handle nonlinear and non-stationary signals. EMD decomposes signals into a set of intrinsic mode functions (IMFs) without predefined bases, while HHT further analyzes these IMFs to extract instantaneous frequencies and their amplitude information that are crucial for fault diagnosis [11, 12]. However, EMD and HHT face issues like mode mixing, end effects, and noise sensitivity, which affect robustness [13, 14]. Variational Mode Decomposition (VMD) improves on these by extracting band-limited modes with optimized center frequencies, producing more stable and noise-robust decompositions. VMD has been effectively utilized for diagnosing bearing and gear faults [15, 16]. However, these methods still struggle to effectively capture the cross-scale internal modulation relationships between amplitude modulation (AM) and frequency modulation (FM), which are essential for defect diagnosis in rotating machinery [17, 18].

Despite their broad use in fault diagnosis, these methods are constrained in their capacity to fully capture the dynamic and intricate behaviors of rotating machinery problems. To address these limitations, the Holo-Hilbert Spectral Analysis (HHSA) method was introduced by Huang et al. in 2016, extending the traditional TFA methods to a higher-order representation [19]. HHSA uses a double-layer nested EMD decomposition structure to create a three-dimensional Holo-Hilbert Spectrum (HHS), which captures both AM and FM components in nonlinear and non-stationary signals. This method has shown significant potential in handling nonlinear, non-stationary data without requiring predefined basis functions, making it highly adaptable for practical fault diagnosis applications. The cross-scale coupling relationship between the AM and FM characteristics of vibration signals is explicated by the HHSA method, improving fault diagnosis accuracy in rotating machinery systems [20]. In comparison with traditional time–frequency and decomposition methods, HHSA offers several substantial improvements by directly addressing their known limitations. Methods such as FFT, Short-Time Fourier Transform (STFT), and WT are constrained by fixed-resolution windows or predefined basis functions, which restrict their ability to characterize multicomponent and time-varying modulation behaviors. EMD- and HHT-based approaches, while adaptive, often suffer from mode mixing, end effects, noise sensitivity, and ambiguity in instantaneous frequency estimation. VMD improves decomposition robustness but requires a predefined number of modes and still falls short in representing cross-scale AM–FM interactions that are essential for fault identification. HHSA alleviates these confounding issues through its nested decomposition structure, which separates slow-varying AM from fast-varying frequency oscillations. This enables clearer isolation of intrinsic components, preserves hierarchical AM–FM coupling, and reduces mode ambiguity. The resulting three-dimensional HHS provides a richer and more interpretable representation of nonlinear and non-stationary vibration responses, overcoming the limitations that hinder conventional methods [20, 21].

Building upon these advanced signal representation capabilities, effective feature extraction is essential for reducing data complexity, suppressing irrelevant noise, and preserving discriminative information for classification. However, accurate fault identification also depends on robust machine learning methods that can learn representative patterns from extracted features and generalize effectively to unseen data. Common classifiers include Logistic Regression, Decision Trees, Random Forests [22], Support Vector Machines (SVMs) [23], K-Nearest Neighbors (KNNs) [24], and Neural Networks [25]. Each method has its strengths and weaknesses. Logistic Regression is easy to understand, but it struggles with nonlinear data. Decision Trees are good at creating clear rules but can easily overfit the data. Random Forests help reduce the problem of variance by averaging the results of many trees [26]. SVMs are effective with data that are both nonlinear and have many dimensions [27]. KNN is simple to use, but it requires a lot of computing power. Deep Neural Networks (DNNs) are effective at finding complex patterns, but they need substantial datasets and considerable computational resources [28].

Prior comparative research has integrated advanced signal techniques with machine learning for defect diagnosis [29–31]. For instance, Niu et al. [29] suggested a hybrid framework combining structural vibration characteristics with lightweight models to improve diagnostic efficiency while maintaining accuracy. Xu and Li [30] introduced an optimized deep belief network enhanced by a sparrow search strategy, demonstrating improved feature learning capability for bearing fault diagnosis. Similarly, Yang et al. [31] developed a hybrid framework integrating improved VMD and convolutional neural network (CNN)-based models, achieving strong performance in complex vibration environments. Beyond these approaches, VMD combined with SVM has demonstrated high accuracy for bearing faults under controlled settings [32]. Discrete WTs with multilayer perceptron neural networks have been employed for the identification and localization of gear failures [33]. Improved CNNs with discrete wavelet decomposition have efficiently identified faults from limited data [34]. Additionally, HHT combined with self-organizing feature mapping neural networks has demonstrated potential in failure diagnostics because of its capacity to extract and discriminate nonlinear, non-stationary features [35].

To mitigate the issue of limited data availability, a few-shot fault diagnosis method for machinery that incorporates multi-scale perception and multi-level feature fusion with image quadrant entropy has demonstrated strong performance in identifying fault patterns from limited samples by effectively integrating spatial–frequency information [36]. This is evidenced by recent investigations that examine entropy-based feature extraction techniques to effectively characterize the dynamic properties of non-stationary signals. As an illustration, a detailed defect diagnosis framework, which employs phase entropy, captures the dynamic features of non-stationary signals, demonstrating enhanced adaptability across diverse operational environments [37]. Furthermore, a multi-modal, multi-scale, and multi-level fusion approach, utilizing quadrant entropy, has been formulated to leverage complementary information derived from various sensing modalities, thereby improving the robustness and accuracy of mechanical failure detection [38]. Consequently, Wang et al. [39] proposed a parameter-optimized permutation entropy method for diagnosing faults in rotating machinery; this approach improves sensitivity to minor fault characteristics and simultaneously increases resistance to noise interference.

Beyond these advancements, recent research across diverse engineering fields has showcased the rapid evolution of advanced modeling and time-series learning methodologies that are also relevant to machinery fault diagnosis. For example, Long Short-Term Memory (LSTM)-attention neural networks have been employed to improve fault diagnosis performance in induction motors by capturing long-term temporal dependencies in vibration and current signals [40]. In addition, fault diagnosis in soft robotic systems has been explored through motion dynamics modeling, further demonstrating the applicability of nonlinear system analysis to flexible and deformable structures [41]. From a methodological perspective, recent reviews of time-series embedding methods provide in-depth insights into modern feature representation strategies for classification tasks [42], while structure-preserving approaches grounded in normal form theory have also been proposed for analyzing complex nonlinear dynamics in power systems [43]. Collectively, these studies reflect a broader shift toward data-driven and nonlinear-dynamics-informed analysis, further reinforcing the relevance of advanced signal representations for vibration-based fault diagnosis.

Despite the substantial progress achieved by existing signal processing and machine learning approaches, several limitations remain. Most current methods focus either on feature extraction or classification independently, lacking a unified framework that effectively combines advanced signal representation with robust and generalizable learning models. In particular, the use of HHSA-derived features in conjunction with multiple machine learning classifiers for rotating machinery fault diagnosis remains insufficiently explored. Although recent studies have demonstrated the potential of HHSA for revealing AM–FM coupling characteristics, its integration into a comparative machine learning framework for automated fault classification has not yet been fully established.

To overcome this gap, this study provides a comprehensive fault diagnosis framework that combines HHSA with multiple machine learning classifiers. By leveraging the ability of HHSA to extract intrinsic amplitude–frequency modulation characteristics from nonlinear and non-stationary vibration signals, the proposed framework attempts to provide a more informative and discriminative feature representation for fault diagnosis. These features are subsequently evaluated using a diverse set of classifiers, including Logistic Regression, Decision Tree, Random Forest, SVM, KNNs, and DNN, in order to assess the robustness and generalizability of the proposed method across different operating conditions.

The main contributions of this study are as follows:

1) An HHSA-based feature extraction pipeline is utilized to effectively capture AM–FM coupling within nonlinear and non-stationary vibration signals.
2) The enhanced discriminative capability of HHSA-derived features is demonstrated through comparison with conventional FFT-based features.
3) The robustness of the proposed framework is proven by six machine learning classifiers using a laboratory-scale dataset covering four operating conditions.

The remainder of this paper is structured as follows. Section 2 describes the dataset, HHSA methodology, feature extraction process, and machine learning classifiers. Section 3 delineates the experimental findings and discussion. Section 4 concludes the study and outlines future research directions.

2. Materials and Methods

Figure 1 presents an overview of the proposed HHSA-based fault diagnosis framework, including vibration data acquisition, signal processing, feature extraction, and classification.

2.1. Dataset description

The experimental vibration dataset utilized in the present research is derived from the publicly available VBL-VA001 lab-scale benchmark, which was specifically designed to emulate typical fault mechanisms encountered in rotating machinery systems. The testbed consists of five electric motors configured to reproduce four representative machine conditions, namely, normal operation, unbalance, misalignment, and bearing fault [44]. These fault conditions were selected to cover the most commonly observed mechanical degradation modes in rotating equipment and to ensure clear physical interpretability of vibration signatures.

The unbalance faults were generated by attaching eccentric masses of 4 g and 18 g at a radius of 1.5 cm on the motor impeller, producing two distinct unbalance severities of 6 g·cm and 27 g·cm, respectively. This configuration enables modeling vibration responses under different rotational mass–eccentricity levels, reflecting practical unbalance conditions occurring in rotating components.

The misalignment condition was created by coupling the motor shaft with an additional metal cylinder offset by 3 mm,

Figure 1
Workflow of the proposed HHSA-based fault diagnosis framework

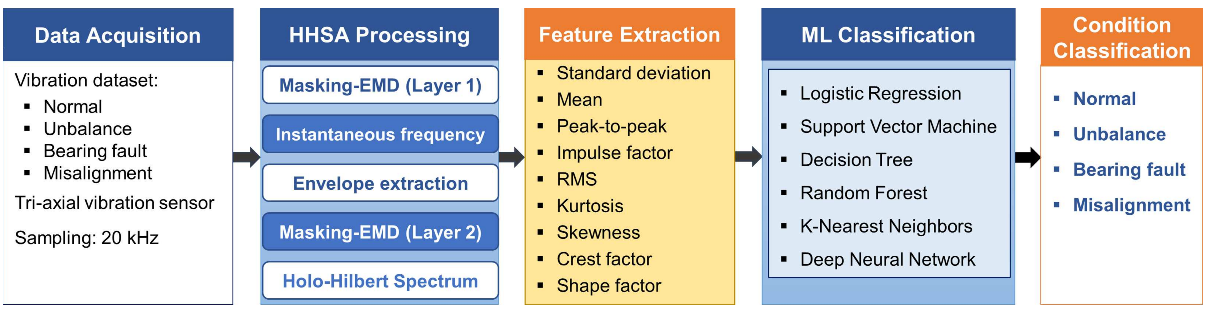

simulating shaft angular and parallel misalignment that commonly arises from improper installation or mechanical wear.

The bearing fault state was initiated through controlled mechanical impacts applied to the outer bearing ring, generating crack-like damage that manifests spectral features detectable on both the inner and outer bearing raceways. This approach allows reproduction of generalized bearing defect patterns rather than isolating single fault types.

Vibration signals were measured using a LOG-0002-100G-DC-8GB-PC tri-axial sensor mounted on a rigid section of the motor casing to minimize structural resonance and signal distortion. Measurements were recorded simultaneously along three orthogonal axes (x, y, z) at a sampling rate of 20 kHz. For each operating condition, vibration data were collected in 5-s segments, with each segment regarded as an independent sample. Prior to analysis, the recorded signals were checked for missing or corrupted values, which were removed. To ensure comparability across different operating conditions, all signals were normalized using a min–max scaling procedure before applying the HHSA. Table 1 summarizes the dataset composition. The dataset is balanced, with 1000 samples collected for each of the four machine conditions. Figure 2 illustrates time-domain vibration signals for the four operating conditions.

Table 1
Description of VBL-VA001 dataset with four machine conditions

Condition type	Class label	Sample number
Normal	1	1000
Unbalance	2	1000
Bearing	3	1000
Misalignment	4	1000

2.2. Holo-Hilbert Spectrum Analysis

Traditional spectral analysis techniques, such as FFT and WT, primarily rely on additive signal decomposition and often require prior assumptions regarding signal stationarity or frequency bands. In contrast, real-world vibration signals from rotating machinery exhibit nonlinear, non-stationary behavior with complex AM and FM coupling. Methods like VMD and HHT, while adaptive, may still overlook cross-scale interactions. This study uses HHSA to address these limitations, enabling simultaneous analysis of AM and FM properties without requiring predefined bases or prior signal assumptions. HHSA utilizes a double-layer nested decomposition structure, which enables comprehensive analysis of cross-scale couplings in vibration signals [19].

This approach allows both intra-mode nonlinear interactions and inter-mode modulations to be analyzed more effectively. Unlike conventional frequency-domain analysis, HHSA offers a multidimensional perspective that simultaneously reveals both frequency and amplitude modulation variations in signals originating from nonlinear and non-stationary systems [45].

To address common issues in EMD, such as mode mixing and endpoint effects, a Masking-EMD scheme is employed within the HHSA framework to improve decomposition robustness [46, 47]. The approach is particularly effective in uncovering complex coupling mechanisms present in nonlinear vibration signals.

A comprehensive overview of the HHSA procedure is presented as follows. The raw vibration signal $v(t)$ is first decomposed into IMFs using the Masking-EMD approach. The decomposition is expressed as:

$$\begin{aligned} v(t) &= \sum_{i=1}^{m} c_i(t) + r(t) \\ &= \sum_{i=1}^{m} a_i(t) \, cos\theta_i(t) + r(t) \end{aligned} \tag{1}$$

where $c_i(t)$ represents the i-th IMF, which is written as $a_i(t)\cos\theta_i(t)$, $a_i(t)$ denoting the amplitude function and $\theta_i(t)$ the instantaneous phase of the i-th IMF. The residual $r(t)$ denotes the non-oscillatory component of the signal and is discarded before statistical feature extraction. The instantaneous frequency (IF) and amplitude function of each IMF are determined using the Direct Quadrature method [48], with the IF defined as the time derivative of the phase $\theta_i(t)$. This frequency is referred to as the “carrier frequency” and is represented on the x-axis of the HHS.

To compute the amplitude function $a_i(t)$ of each IMF, the absolute value of the IMF is first calculated. The local maxima of this absolute value are then identified [19]. A natural cubic spline interpolation is applied to construct a smooth envelope passing through these maxima, defining the amplitude function $a_i(t)$ and capturing the instantaneous variations in the amplitude of the signal.

The amplitude function of each IMF is then further decomposed to extract detailed AM features. The amplitude function $a_i(t)$ is decomposed into second-layer IMFs as:

$$a_i(t) = \sum_{j=1}^{n} a_{ij}(t) \, cos\beta_{ij}(t) + r_{ij}(t) \tag{2}$$

Thus, $v(t)$ can be noted as Eq. 3:

$$v(t) = \sum_{i=1}^{m} \left(\sum_{j=1}^{n} a_{ij}(t) \, cos\beta_{ij}(t) + r_{ij}(t) \right) cos\theta_i(t) + r(t) \tag{3}$$

where $a_{ij}(t)$ denotes the second-layer amplitude function, $\beta_{ij}(t)$ represents the second-layer phase function, and $r_{ij}(t)$ signifies the second-layer trend associated with the second-layer IMF. The corresponding instantaneous “AM frequency” is expressed as the time derivative of the second-layer phase function, $\beta_{ij}(t)$. This step is referred to as “AM expansion,” which involves broadening each first-layer amplitude function into AMs across diverse temporal scales.

Finally, the HHS is constructed by integrating the modulation energy over all time points for both the carrier frequency and the AM frequency. This integration results in the two-dimensional power distribution across both the carrier and AM frequencies. The HHS is obtained, where the x-axis represents the carrier frequency, the y-axis represents the modulation frequency, and the color map indicates the distribution of modulation energy across the frequency dimensions.

Figure 3 illustrates the HHSA workflow utilized for a vibration signal from the normal operating condition. As illustrated in Figure 3(a), the vibration signal is initially decomposed employing the Masking-EMD, which extracts a set of IMFs that capture the dominant FM components of the signal, as presented in Figure 3(b). Among these, IMF3 is selected for further analysis. The instantaneous frequency of IMF3, obtained via the Hilbert transform, is depicted in Figure 3(c), while its amplitude envelope is shown in Figure 3(d). To analyze AM characteristics, the

Figure 2
Example vibration signals in three axes for four machine conditions (normal, unbalance, bearing fault, and misalignment)

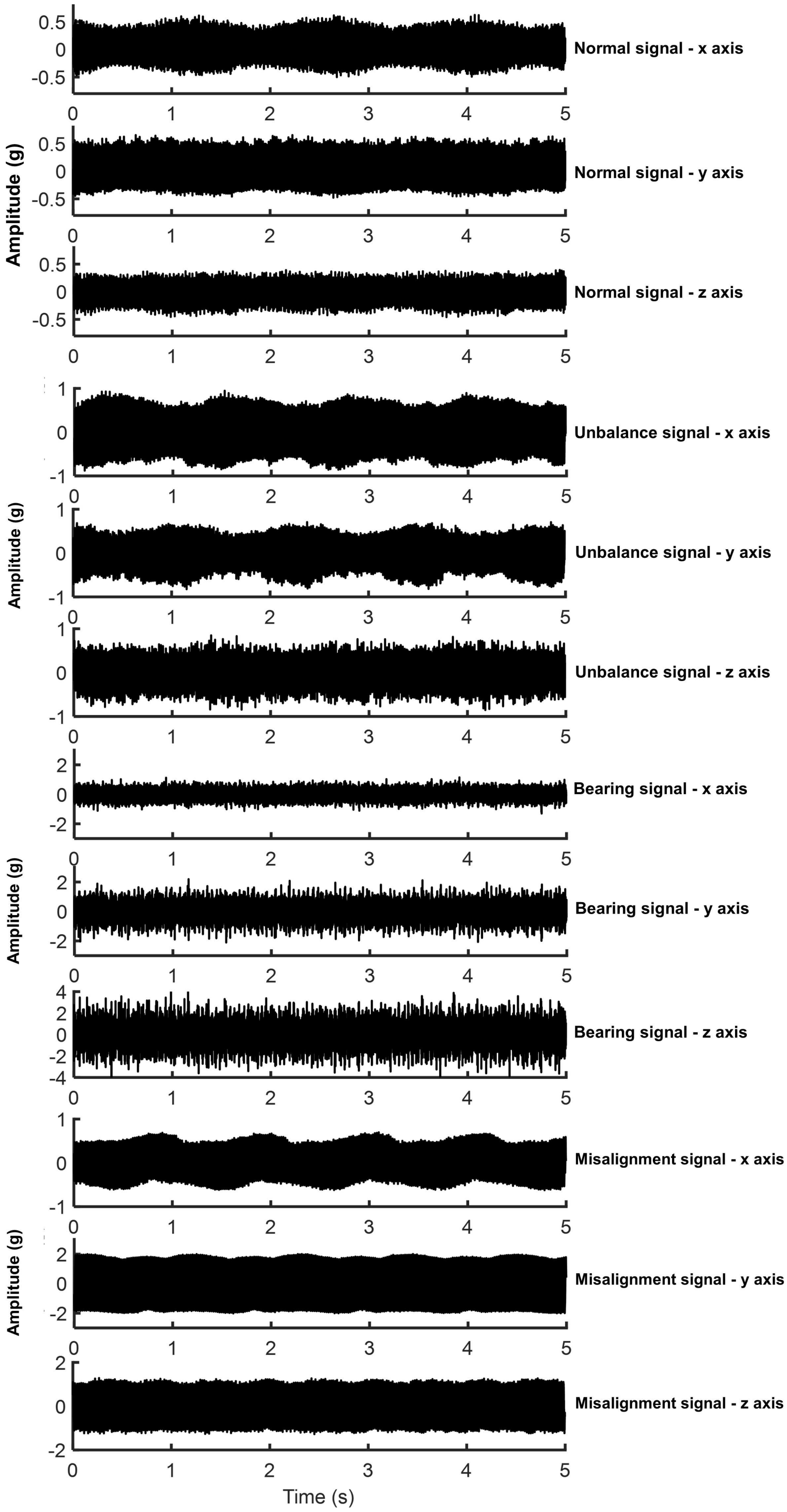

Figure 3
HHSA-based vibration signal analysis process

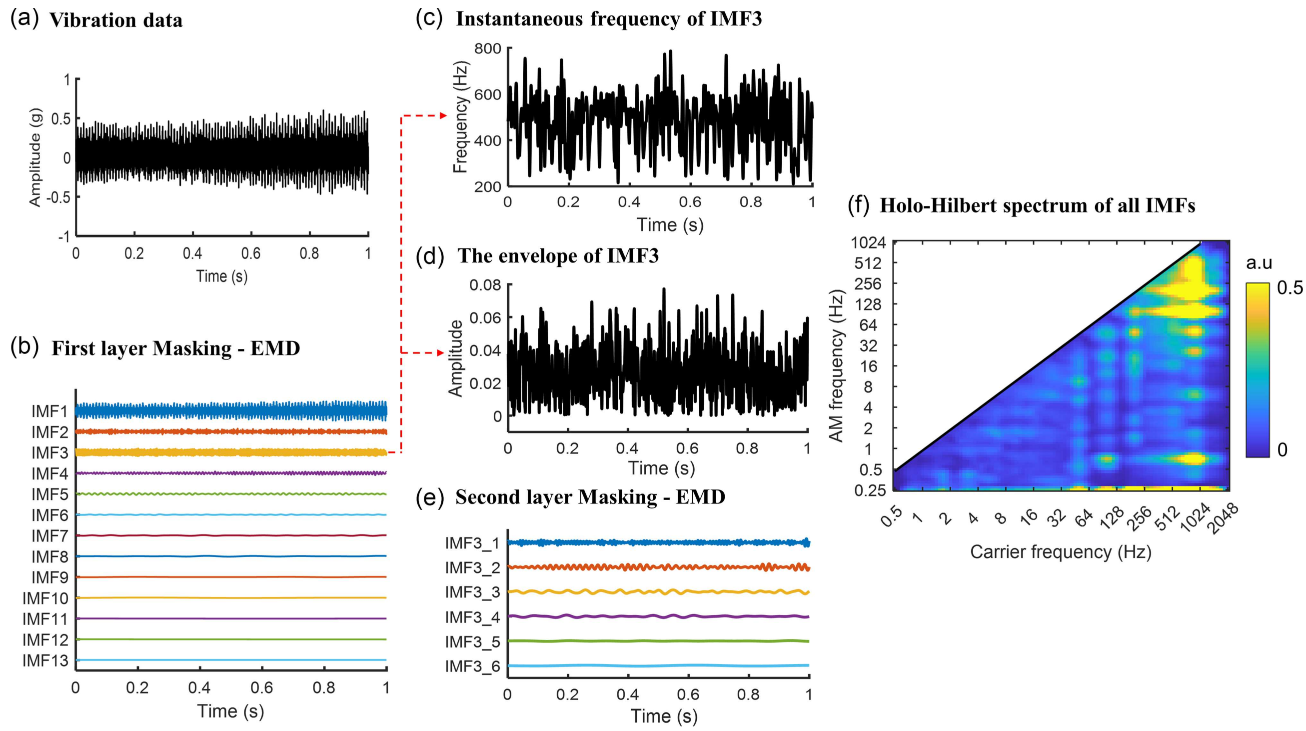

envelope of IMF3 is subjected to a second-layer Masking-EMD, resulting in multiple second-layer IMFs that reveal various AM modes, as illustrated in Figure 3(e). Subsequently, each second-layer IMF is processed using the Hilbert transform to extract its instantaneous AM frequency. The final HHS, shown in Figure 3(f), is constructed by integrating the modulation energy across time for all combinations of carrier and AM frequencies. The HHS exhibits concentrated energy at 512–1024 Hz carrier frequencies with AM components (90–512 Hz). This two-dimensional representation enables the joint characterization of AM and FM components, providing a comprehensive view of the underlying nonlinear and non-stationary dynamics. The diagonal energy pattern observed in the HHS highlights the presence of strong coupling between carrier and modulation frequencies.

This analysis pipeline is applied consistently to all fault categories in the dataset. The resulting HHSA spectra for misalignment, bearing fault, and unbalance are displayed in Figure 4 for direct visual comparison of their AM–FM coupling characteristics. Misalignment is characterized by dominant energy at lower carrier frequencies (64–256 Hz) with AM components in the 50–128 Hz range. Bearing faults produce broadband energy extending up to 2000 Hz with AM components spanning 16–1024 Hz, while unbalance is dominated by energy at 128–1024 Hz carrier frequencies with AM components in the 40–512 Hz range. These distinct AM–FM distributions reflect unique vibration signatures for each fault condition.

2.3. Extracted features

In the current study, statistical features were retrieved from the HHS to characterize the vibration signals. The HHS provides a two-dimensional representation of signal energy distribution over carrier and modulation frequencies, enabling comprehensive analysis of both time-varying and frequency-varying behaviors.

Feature extraction was performed over the entire HHS rather than selected frequency bands. This full-spectrum approach ensures that both low- and high-frequency components are captured, preserving critical information that may be distributed across different frequency regions. As a result, it avoids potential information loss associated with band-limited analysis and provides a more holistic representation of signal characteristics.

To reduce data dimensionality while retaining essential information, a set of statistical descriptors was computed from the HHS, including mean, standard deviation, Root Mean Square (RMS), peak-to-peak, impulse factor, skewness, kurtosis, crest factor, and shape factor [49, 50]. These features form a compact representation of the signal and serve as inputs for machine learning classification. Additionally, this approach eliminates the need for manual frequency band selection, thereby simplifying the analysis procedure and improving robustness.

Table 2 presents the mean normalized feature values for the four operating conditions: normal, unbalance, bearing fault, and misalignment. All features were standardized using z-score normalization prior to classification; therefore, the reported values represent normalized quantities rather than physical measurements. The results indicate that the unbalance condition exhibits the highest impulse factor, reflecting stronger high-amplitude transient components, whereas the normal condition shows relatively low skewness and kurtosis, suggesting a more stable and symmetric energy distribution. These differences confirm the strong discriminative capability of the HHSA-derived features.

1) Feature visualization using t-SNE

To further assess the effectiveness of the collected features, t-SNE (t-distributed Stochastic Neighbor Embedding) was utilized for visualization. This dimensionality reduction technique

Figure 4
Holo-Hilbert spectra of misalignment, bearing fault, and unbalance

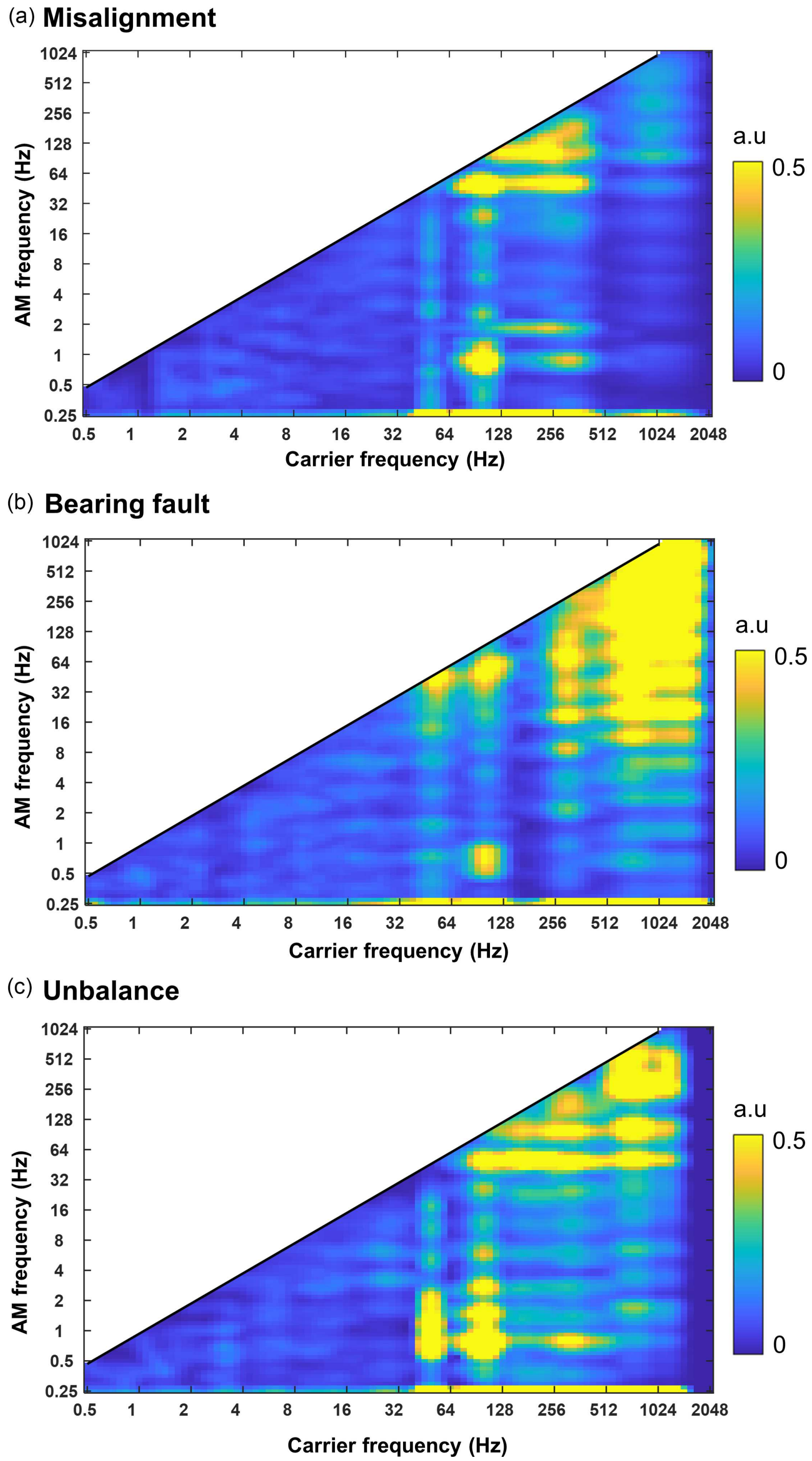

Table 2
Statistical features extracted from the HHS for each machine condition

Conditions	Mean	Standard deviation	RMS	Peak to peak	Impulse factor	Skewness	Kurtosis	Crest factor	Shape factor
Normal	–1.180	–0.868	–0.953	–1.125	–0.812	–0.967	–0.820	–0.491	–1.109
Unbalance	1.336	1.503	1.133	1.459	1.586	1.285	0.891	1.042	1.062
Bearing fault	–0.096	–0.029	0.280	–0.117	–0.088	0.354	0.151	0.103	0.606
Misalignment	–0.061	–0.606	–0.460	–0.217	–0.687	–0.672	–0.222	–0.654	–0.559

is intended to depict high-dimensional data in two- or three-dimensional space. Applying t-SNE to the feature vectors derived from the full HHS made it possible to examine how distinctly the fault conditions were separated in feature space.

The t-SNE visualization revealed that the features extracted from the HHS resulted in clear separability between the various fault types, such as normal, unbalance, bearing, and misalignment. The minimal overlap between the clusters indicates the strong discriminative power of the HHS features. This visualization provides additional confirmation of the capacity of the extracted features to effectively distinguish across different machine conditions.

2.4. Machine learning classifiers

In the current study, six widely used machine learning classifiers were utilized to assess the efficacy of the features extracted using HHSA. These classifiers span different modeling approaches, from linear models to nonlinear and ensemble techniques, providing an extensive assessment of the proposed fault diagnosis framework. Each classifier was fine-tuned through hyperparameter optimization to achieve the best classification performance.

1) Logistic Regression

Logistic Regression is a highly effective and widely recognized method for supervised classification [51]. It estimates class probabilities by learning linear decision boundaries and offers strong interpretability. The probability of class membership is expressed as:

$$P(y = 1|x) = \frac{1}{1 + e^{-(w^T x + b)}} \tag{4}$$

where x is the input feature vector, w is the weight vector, and b is the bias term. In this study, Logistic Regression was extended to the four-class fault diagnosis problem using an error-correcting output codes (ECOC) multiclass strategy. The regularization strength (λ) was optimized via Bayesian search to mitigate overfitting and enhance generalization.

2) Support Vector Machine

SVM seeks to determine an optimal hyperplane that maximizes the separation between data points of disparate classes in a high-dimensional feature space [52]. The decision function can be written as:

$$f(x) = \sum_{i=1}^{N} \alpha_i y_i K(x_i, x) + b \tag{5}$$

where $K(x_i, x)$ is the kernel function. The Radial Basis Function kernel was adopted to capture nonlinear relationships inherent in HHSA-derived features. In this study, SVM was extended to the four-class fault diagnosis problem using an ECOC multiclass strategy. Hyperparameters, such as the box constraint C and kernel scale, were optimized using Bayesian methods to enhance boundary flexibility and classification performance.

3) Decision Tree classifier

The Decision Tree is a fundamental and widely utilized machine learning technique, particularly effective for classification tasks [53]. It recursively partitions the feature space by minimizing node impurity, commonly measured by the Gini index:

$$Gini = 1 - \sum_{k=1}^{K} p_k^2 \tag{6}$$

where p_k is the proportion of samples belonging to class k in a given node. Although prone to overfitting, its performance can be significantly improved with proper hyperparameter tuning. This study improved the maximum number of splits and the minimum leaf size to achieve a balance between model complexity and generalization.

4) Random Forest

Random Forest is an ensemble learning technique that generates many decision trees from bootstrapped data samples and aggregates their predictions through majority voting [51]. The final prediction is given by:

$$\hat{y} = mode\{h_1(x), h_2(x), \ldots, h_T(x)\} \tag{7}$$

where $h_t(x)$ denotes the prediction of the t-th tree. This approach reduces variance and improves robustness, making it effective for high-dimensional HHSA features. The quantity of trees and number of predictors sampled per split were optimized using a Bayesian search to achieve superior performance.

5) K-Nearest Neighbors

KNN is a non-parametric, instance-based learning method commonly utilized for classification purposes. KNN classifies a new data point by determining the predominant class of its k nearest neighbors in the feature space [51].

$$\hat{y} = mode\{y_i | x_i \in N_k(x)\} \tag{8}$$

where $N_k(x)$ denotes the set of the K nearest neighbors of sample x. Its efficacy is contingent upon the selection of distance metric and neighborhood size. Hence, Bayesian optimization was used to ascertain the ideal number of neighbors and distance function.

6) Deep Neural Network

A DNN comprises several layers of neurons, with each layer processing the incoming data using learning weights and activation functions [54]. The transformation at layer l can be expressed as:

$$a^{(l)} = \sigma(W^{(l)} a^{(l-1)} + b^{(l)}) \tag{9}$$

where $W^{(l)}$and $b^{(l)}$ are the weight matrix and bias vector of layer l, respectively, and σ is the activation function. The Adam optimizer and early stopping were employed to improve convergence and mitigate overfitting. Although not tuned via Bayesian optimization, key architectural hyperparameters (number of neurons, dropout ratios, learning rate, and batch size) were selected through systematic experimentation to ensure stable performance.

2.5. Hyperparameter optimization

To ensure fair and consistent comparison across classifiers, Bayesian optimization was used for Logistic Regression, SVM, Decision Tree, Random Forest, and KNN, combined with 5-fold cross-validation. Bayesian optimization efficiently explores the hyperparameter search space and avoids overfitting by leveraging probabilistic surrogate models. For each classifier, the optimal configuration was determined based on validation accuracy and then retrained on the complete training data of each fold. The resulting optimal hyperparameters are listed in Table 3.

2.6. Evaluation metrics

To assess the classifiers' performance in this work, several evaluation metrics were employed to quantify how well each model performed in diagnosing faults in rotating machinery. These metrics are based on the model's predictions and provide a comprehensive understanding of their classification capabilities. The following metrics were calculated for each classifier:

1) Accuracy

Accuracy represents the proportion of successfully classified samples over the total number of predictions. It provides the overall performance of the model and is defined as:

$$Accuracy = \frac{TP + TN}{TP + TN + FP + FN} \tag{10}$$

2) Precision

Precision measures the proportion of predicted positive samples that are truly positive. This metric becomes particularly important when false alarms must be minimized. In fault diagnosis, a high precision value indicates that the model is reliable when identifying fault conditions. Precision is computed as:

$$Precision = \frac{TP}{TP + FP} \tag{11}$$

3) Recall

Recall assesses the model's ability to correctly identify actual positive cases. It is especially important when missing a fault (false negative) is costly. A high recall value indicates that most fault instances are successfully detected. Recall is given by:

$$Recall = \frac{TP}{TP + FN} \tag{12}$$

4) F1-Score

The **F1-score** offers a balanced evaluation by integrating precision and recall into a single metric through their harmonic mean. It is especially useful for imbalanced datasets, where both false positives and false negatives need to be considered. The F1-score is computed as:

$$F1 - score = 2\frac{Precision \times Recall}{Precision + Recall} \tag{13}$$

3. Results and Discussion

The experimental results of this study demonstrate that combining HHSA with various machine learning classifiers yields excellent performance in fault diagnosis for rotating machinery. Table 4 summarizes the classification efficacy of six distinct classifiers, assessed through 5-fold cross-validation with Bayesian hyperparameter optimization. All reported results correspond to the mean values obtained from five-fold cross-validation, which is adopted to reduce performance variance and enhance the statistical reliability of the evaluation. Logistic Regression, Random Forest, and KNN achieved near-perfect performance across all evaluation metrics—accuracy, precision, recall, and F1-score. These results highlight the robustness of HHSA-derived features, indicating that even relatively simple models can achieve near-perfect classification performance. This also demonstrates

Table 3
Optimized hyperparameters for machine learning classifiers

Classifier	Key hyperparameters	Optimized values
Logistic Regression	Regularization type; Lambda	L2 (ridge); 6.6745×10^{-5}
Decision Tree	MaxNumSplits; MinLeafSize	164; 6
Random Forest	NumLearningCycles; NumVariablesToSample	104; 3
K-Nearest Neighbors	NumNeighbors; Distance metric	1; Standardized Euclidean
Support Vector Machine	BoxConstraint (C); KernelScale	933.57; 57.674
Deep Neural Network	NumHiddenUnits1; Dropout1; NumHiddenUnits2; Dropout2; LearnRate; BatchSize	64; 0.196; 17; 0.331; 0.0045; 62

Table 4
Classification performance of six machine learning models using HHSA-based features

Classifier	Accuracy (%)	Precision (%)	Recall (%)	F1-score (%)
Logistic Regression	99.95	99.95	99.95	99.95
Decision Tree	99.83	99.83	99.83	99.82
Random Forest	99.95	99.95	99.95	99.95
Support Vector Machine	99.92	99.93	99.92	99.92
K-Nearest Neighbors	99.95	99.95	99.95	99.95
Deep Neural Network	99.92	99.93	99.92	99.92

the versatility of the proposed method across different machine learning classifiers.

In terms of precision, Logistic Regression, KNN, and Random Forest achieved 99.95%, indicating minimal false positives and suggesting that the models are highly reliable for fault diagnosis. Similarly, recall values also reached 99.95%, indicating the classifiers' effectiveness in detecting almost all fault instances, thereby minimizing false negatives. The F1-score, which balances precision and recall, also achieved 99.95% across these classifiers, further validating their ability to accurately identify fault conditions.

While Decision Trees showed a slight drop in performance with 99.83% accuracy, the model still achieved impressive results with 99.83% precision, 99.83% recall, and 99.82% F1-score, reinforcing the effectiveness of the HHSA-based framework. Decision Trees are prone to overfitting, especially with deep trees, but the results indicate that HHSA features help maintain a good balance between precision and recall, preventing significant overfitting.

The SVM and DNN classifiers both achieved 99.92% accuracy and similarly high values for precision (99.93%), recall (99.92%), and F1-score (99.92%), demonstrating their effectiveness in handling complex fault conditions. These results indicate that HHSA features are not only suitable for simpler models but also enhance the performance of models requiring higher complexity in learning and decision-making. For comparison, Table 5 reports the classification results using FFT-based features under identical experimental conditions. While both methods achieved high accuracy, HHSA consistently outperformed FFT across all classifiers. For example, Decision Tree improved from 99.72% with FFT to 99.83% with HHSA, while Random Forest increased from 99.90% to 99.95%. Although the absolute differences appear small, such improvements are critical in practical fault diagnosis, where even minor reductions in false alarms or missed detections can translate into substantial operational benefits. These results confirm that HHSA provides a more discriminative and noise-resilient feature set than FFT, owing to its ability to capture the joint time–frequency modulation characteristics of vibration signals.

Figure 5 presents the confusion matrices of the six classifiers—Logistic Regression, SVM, Decision Tree, Random Forest, KNN, and DNN—based on HHSA-extracted features. These results correspond to the final fold of the 5-fold cross-validation process and serve as a representative example of model performance. All classifiers achieved excellent classification accuracy on this test fold, with most models providing perfect classification across the four operating conditions: normal, unbalance, bearing fault, and misalignment. Minor misclassifications were observed in the SVM and DNN models, each showing a 0.5% error rate due to a single misclassified sample. Importantly, these errors were isolated and did not consistently occur between the same fault types, suggesting that they are random rather than systematic (e.g., not repeated confusion between misalignment and unbalance). This further supports the robustness of HHSA features in avoiding bias toward specific fault categories.

The fact that both simple classifiers like Logistic Regression and KNN, as well as more sophisticated models like SVM and DNN, achieved comparable high performance highlights the versatility of HHSA features. This indicates that HHSA is adaptable across many machine learning algorithms, providing a solid feature set to improve classification performance regardless of model complexity. This versatility makes HHSA a compelling option for fault diagnosis in industrial environments, where computational resources, real-time performance, and interpretability are often key considerations.

Compared to FFT, which primarily analyzes signals in the frequency domain under assumptions of stationarity, HHSA offers a significant advantage in managing non-stationary and nonlinear vibration signals. In our experiments, FFT-based

Table 5
Classification performance of six machine learning models using FFT-based features

Classifier	Accuracy (%)	Precision (%)	Recall (%)	F1-score (%)
Logistic Regression	99.95	99.95	99.95	99.95
Decision Tree	99.72	99.73	99.72	99.72
Random Forest	99.90	99.90	99.90	99.90
SVM	99.92	99.93	99.92	99.92
KNN	99.90	99.90	99.90	99.90
DNN	99.83	99.83	99.83	99.82

Figure 5
Confusion matrices of classification results using HHSA-based features for four fault conditions (normal, unbalance, bearing fault, and misalignment) across different classifiers

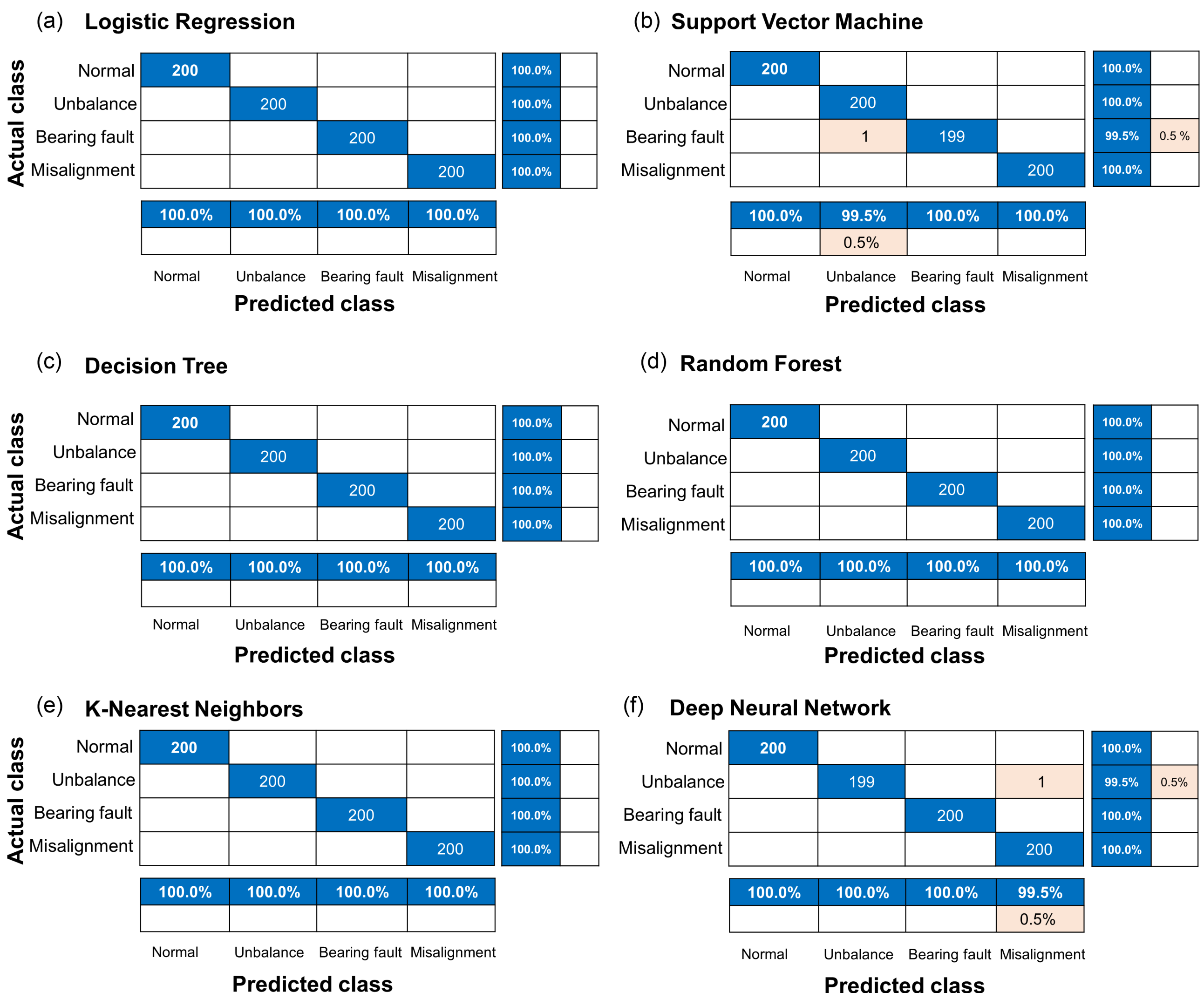

features (Table 5) also achieved very high accuracy, with the best result reaching 99.95% for Logistic Regression, surpassing the 99.75% accuracy reported in previous FFT-based studies [44]. However, FFT performance varied more across classifiers, with Decision Trees and DNN showing slightly lower accuracy (99.72–99.83%). In contrast, HHSA-based features (Table 4) provided consistently near-perfect results across all classifiers, indicating stronger robustness and generalizability. This consistency highlights HHSA's ability to capture the dynamic AM–FM characteristics of vibration signals, rendering it a more reliable feature extraction method for various machine learning methods.

To further evaluate the discriminative power of HHSA-derived features, t-SNE was applied for feature visualization. Figure 6 presents the clustering of the test set in two dimensions, showing four distinct groups corresponding to normal, unbalance, bearing, and misalignment. The clusters are well-separated, indicating that HHSA features provide a highly discriminative representation of the vibration data.

Notably, the few misclassified samples observed in SVM and DNN—each corresponding to a single sample in Table 4—appear near the boundaries of their respective clusters in the t-SNE plot. This observation suggests that these minor errors are primarily due to ambiguous feature representations where different fault types exhibit partial overlap, rather than deficiencies in the HHSA feature extraction itself. In other words, HHSA

Figure 6
t-SNE visualization of HHSA-extracted features

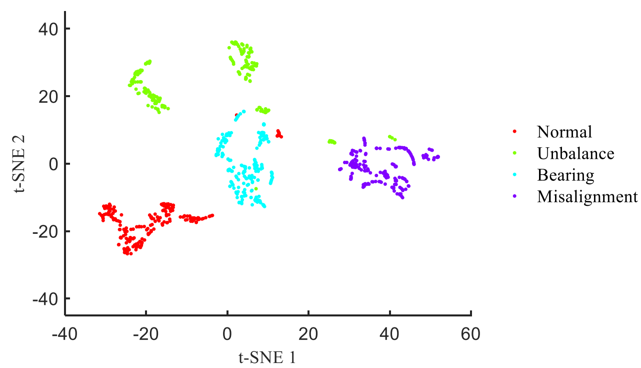

successfully captures the amplitude–frequency modulation characteristics of the signals, and classification errors arise in regions where the underlying feature distributions are intrinsically less separable.

The overall strong separation of clusters, coupled with the minimal number of boundary samples, supports the robustness and efficacy of HHSA features for defect detection. These visual insights align with the high classification accuracies reported across all models, confirming that HHSA provides a reliable feature set for distinguishing between different fault conditions, even when minor ambiguities exist in the data.

Beyond FFT, various advanced signal decomposition and TFA techniques have been explored for rotating machinery fault diagnosis, and a qualitative comparison with these approaches provides important context for evaluating the proposed HHSA-based framework, including the STFT, WT, HHT, and VMD integrated with machine learning or deep learning classifiers [55, 56]. While these approaches have achieved considerable success, each has limitations when applied to nonlinear and non-stationary vibration signals, particularly under high noise levels and variable operating conditions. STFT and WT, constrained by the Heisenberg–Gabor limit, provide fixed or semi-fixed resolution, resulting in coarse spectral representations for rapidly varying features. HHT improves adaptivity but cannot fully capture cross-scale AM–FM coupling [57]. VMD offers better mode separation and noise resistance than EMD but requires sensitive parameter tuning [48]. Similarly, WT-based methods depend heavily on the careful selection of wavelet type and decomposition levels [58].

In the context of bearing defect diagnosis, Ying et al. [18] performed a comprehensive comparison of HHSA with HHT, Continuous Wavelet Transform (CWT), and Short-Time Fourier Transform (STFT) using both simulated and experimental data under strong noise conditions. Their results demonstrated that HHSA could distinctly reveal the coupling between carrier frequencies and modulation frequencies—including fundamental fault frequencies and harmonics—while other TFA methods either failed to detect sidebands or produced blurred time–frequency representations. Moreover, HHSA maintained robust feature extraction in Gaussian white noise environments and outperformed envelope spectrum analysis and first-order Masking-EMD in preserving fault-related AM–FM characteristics.

The performance of HHSA stems from its double-layer EMD framework, which inherently separates AM and FM components without requiring predefined bases or extensive parameter tuning. This enables the generation of a full informational spectrum—HHS—that clearly represents the internal modulation relationship between frequency scales. In our study, these advantages translated into stable and accurate fault feature extraction across varying operating conditions. This is consistent with the signal-level observations reported by Ying et al. [18], who validated the effectiveness of HHSA in producing discriminative spectral representations. However, unlike Ying et al., who focused only on spectrum analysis without integrating AI classifiers, our work extends HHSA into a machine learning framework, thereby achieving more robust and automated fault diagnosis suitable for industrial applications

3.1. Limitations and future work

Despite the promising performance of the proposed HHSA-based fault diagnosis framework, several limitations remain that warrant further investigation. First, the dataset employed in the present research was gathered under controlled laboratory conditions and includes only four operating conditions—normal, unbalance, bearing fault, and misalignment. Although these represent common fault types, they do not fully capture the diversity, severity levels, and operational variability encountered in real industrial machinery, where factors such as fluctuating load, speed changes, and environmental disturbances may significantly influence vibration responses. Expanding the dataset to include additional fault modes, varying fault severities, and measurements from real-world operating conditions is therefore essential for enhancing the framework's generalizability.

Second, while the results demonstrate that HHSA-derived features provide higher or comparable accuracy relative to FFT-based features, systematic benchmarking against a broader set of feature extraction methodologies—such as VMD, STFT, WT, and HHT—remains limited. A comprehensive comparison under identical testing conditions, including robustness to noise and environmental interference, would allow a more rigorous assessment of the diagnostic advantages of the HHSA representation in industrial settings.

Third, the current study includes a shallow DNN as one of the classifiers; however, this architecture is relatively simple when compared with cutting-edge deep learning models. Future study should investigate the use of more advanced architectures like CNNs, Recurrent Neural Networks, or transformer-based models, which may better capture spatial–frequency patterns, long-term temporal dependencies, or contextual modulation structures present in HHSA-derived representations. Such models may further enhance diagnostic accuracy, particularly for large-scale or complex datasets.

Fourth, although HHSA provides a rich characterization of nonlinear AM–FM modulation, its nested EMD structure incurs significant computing complexity, potentially limiting real-time implementation. Future work should explore strategies to accelerate HHSA—such as fast or approximate EMD variants, parallel implementations, or hardware-assisted computation on embedded platforms (e.g., Field-Programmable Gate Array (FPGA), Graphics Processing Unit (GPU), or edge AI processors). Evaluating the end-to-end latency of the diagnostic pipeline will also be necessary to determine suitability for high-frequency, real-time monitoring applications.

Finally, integrating the proposed framework into industrial predictive maintenance systems will require additional validation under diverse operational conditions, including variable speeds, fluctuating loads, and noisy environments. Future research should also investigate sliding-window or streaming implementations of HHSA, online model updating, and the incorporation of explainable AI techniques to improve interpretability and user acceptance in industrial environments.

4. Conclusion

This study proposes a practical and accurate fault diagnosis framework for rotating machinery by combining HHSA with six widely used machine learning classifiers. Experimental results show that HHSA-derived features are highly discriminative, enabling precise classification of multiple fault conditions and attaining near-perfect accuracy, precision, recall, and F1-scores across all models. Interestingly, simpler classifiers such as Logistic Regression and KNN performed comparably to more complex models like SVM and DNN, highlighting the versatility and efficiency of the suggested feature extraction method.

Under the evaluated conditions, HHSA achieved slightly higher or comparable performance than FFT-based features across all classifiers. This result indicates that while HHSA is particularly effective in capturing the amplitude–frequency modulation characteristics of non-stationary vibration signals, FFT can still provide competitive performance under certain conditions. Therefore, HHSA offers a reliable and robust alternative for fault feature extraction, with advantages in noise resilience and interpretability for complex or non-stationary signals.

Overall, the proposed HHSA-based framework provides a robust and scalable foundation for fault diagnosis in rotating machinery. Its adaptability to both simple and complex classifiers, combined with reliable performance on non-stationary vibration data, makes it suitable for industrial condition monitoring and predictive maintenance. Future endeavors will concentrate on augmenting the dataset to cover more diverse fault types and operating conditions, benchmarking against alternative feature extraction methods, and optimizing the HHSA pipeline for real-time deployment and improved interpretability.

Acknowledgment

This work was supported by the Ho Chi Minh City University of Technology and Education, Vietnam.

Ethical Statement

This study does not contain any studies with human or animal subjects performed by any of the authors.

Conflicts of Interest

The authors declare that they have no conflicts of interest to this work.

Data Availability Statement

The VBL-VA001 datasets that support the findings of this study are openly available at https://doi.org/10.1007/s42417-023-00959-9, reference number [44].

Author Contribution Statement

Van-Trung Nguyen: Conceptualization, Methodology, Software, Validation, Formal analysis, Investigation, Data curation, Writing - original draft, Writing - review & editing, Visualization. **Ba-Tan Le:** Investigation, Data curation, Writing - original draft, Writing - review & editing. **Van-Phuong Dao:** Methodology, Validation, Writing - review & editing.

References

[1] Zhu, Z., Lei, Y., Qi, G., Chai, Y., Mazur, N., An, Y., & Huang, X. (2023). A review of the application of deep learning in intelligent fault diagnosis of rotating machinery. *Measurement*, *206*, 112346. https://doi.org/10.1016/j.measurement.2022.112346

[2] Chen, H., Li, J.-M., Wang, X.-B., Yu, L.-Q., & Yang, Z.-X. (2025). Review of intelligent fault diagnosis for rotating machinery under imperfect data conditions. *Expert Systems with Applications*, *285*, 127726. https://doi.org/10.1016/j.eswa.2025.127726

[3] Zhang, T., Chen, J., Li, F., Zhang, K., Lv, H., He, S., & Xu, E. (2022). Intelligent fault diagnosis of machines with small & imbalanced data: A state-of-the-art review and possible extensions. *ISA Transactions*, *119*, 152–171. https://doi.org/10.1016/j.isatra.2021.02.042

[4] Salunkhe, V. G., Khot, S. M., Jadhav, P. S., Yelve, N. P., & Kumbhar, M. B. (2024). Experimental investigation using robust deep VMD-ICA and 1D-CNN for condition monitoring of roller element bearing. *Journal of Computing and Information Science in Engineering*, *24*(12), 124501. https://doi.org/10.1115/1.4066595

[5] Wang, C., Jiang, W., Shi, L., & Zhang, L. (2025). Rolling bearing remaining useful life prediction using deep learning based on high-quality representation. *Scientific Reports*, *15*(1), 8228. https://doi.org/10.1038/s41598-025-93165-4

[6] Randall, R. B., & Antoni, J. (2011). Rolling element bearing diagnostics—A tutorial. *Mechanical Systems and Signal Processing*, *25*(2), 485–520. https://doi.org/10.1016/j.ymssp.2010.07.017

[7] Kankar, P. K., Sharma, S. C., & Harsha, S. P. (2011). Fault diagnosis of ball bearings using machine learning methods. *Expert Systems with Applications*, *38*(3), 1876–1886. https://doi.org/10.1016/j.eswa.2010.07.119

[8] Antoni, J. (2006). The spectral kurtosis: A useful tool for characterising non-stationary signals. *Mechanical Systems and Signal Processing*, *20*(2), 282–307. https://doi.org/10.1016/j.ymssp.2004.09.001

[9] Zheng, X., Lei, Z., Feng, Z., & Chen, L. (2024). Legendre Multiwavelet transform and its application in Bearing Fault Detection. *Applied Sciences*, *14*(1), 219. https://doi.org/10.3390/app14010219

[10] Qu, J., Cheng, X., Liang, P., Zheng, L., & Ma, X. (2023). Fault diagnosis of bearings using wavelet packet energy spectrum and SSA-DBN. *Processes*, *11*(7), 1875. https://doi.org/10.3390/pr11071875

[11] Pavithra, R., & Ramachandran, P. (2025). Predictive machine health monitoring using deep convolution neural network for noisy vibration signal of rotating machine using empirical mode decomposition. *Discover Applied Sciences*, *7*(4), 247. https://doi.org/10.1007/s42452-025-06650-w

[12] Indragandhi, V., Kumar, R. S., & Saranya, R. (2024). Hilbert-Huang Transform and machine learning based electromechanical analysis of induction machine under power quality disturbances. *Results in Engineering*, *24*, 103075. https://doi.org/10.1016/j.rineng.2024.103075

[13] Huang, H.-P., Wei, S.-Y., Chao, H.-H., Hsu, C. F., Hsu, L., & Chi, S. (2019). An investigation study on mode mixing separation in empirical mode decomposition. *IEEE Access*, *7*, 100684–100691. https://doi.org/10.1109/ACCESS.2019.2930543

[14] Nguyen, N. V., Nguyen, X. V., & Nguyen, V. T. (2026). Correlation-guided CEEMDAN denoising of in-cylinder combustion pressure signals. *Results in Engineering*, *30*, 110293. https://doi.org/10.1016/j.rineng.2026.110293

[15] Qiao, M., Tang, X., Liu, Y., & Yan, S. (2021). Fault diagnosis method of rolling bearings based on VMD and MDSVM. *Multimedia Tools and Applications*, *80*(10), 14521–14544. https://doi.org/10.1007/s11042-020-10411-9

[16] Ma, Z., & Zhang, Y. (2025). A study on rolling bearing fault diagnosis using RIME-VMD. *Scientific Reports*, *15*(1), 4712. https://doi.org/10.1038/s41598-025-89161-3

[17] W.-K, Wu., T.-Y, Hsu., H.-T, . . . , & Shyu, K.-K. (2022). Study of heart-rate variability in a video task using Holo-Hilbert spectral analysis. In *Biomedical Signal Processing and Control* (*71*, 103229.Lee, T.-M., Lee, P.-L., Lee, I.-H., Lee: https://doi.org/10.1016/j.bspc.2021.103229

[18] Ying, W., Zheng, J., Pan, H., Liu, Q., & Tong, J. (2023). Use of Holo-Hilbert spectral analysis to reveal the amplitude modulation features of faulty rolling bearing signals. *Journal of Vibration and Control*, *29*(21-22), 5067–5077. https://doi.org/10.1177/10775463221130821

[19] Huang, N. E., Hu, K., Yang, A. C., Chang, H.-C., Jia, D., Liang, W.-K., . . . , & Wu, Z. (2016). On Holo-Hilbert spectral analysis: A full informational spectral representation for nonlinear and non-stationary data. *Philosophical Transactions of the Royal Society A: Mathematical, Physical and Engineering Sciences*, *374*(2065), 20150206. https://doi.org/10.1098/rsta.2015.0206

[20] Zheng, J., Ying, W., Pan, H., & Feng, K. (2023). Holo-hilbert square spectral analysis: A new fault diagnosis tool for rotating machinery health management. *Mechanical Systems and Signal Processing*, *189*, 110069. https://doi.org/10.1016/j.ymssp.2022.110069

[21] Huang, N. E., Yuan, W., Juan, C.-H., Liang, W.-K., Wang, Y.-H., Wu, Z., . . . , & Qiao, F. (2025). On the reliability index of the Holo-Hilbert Spectral Analysis. *Advances in Data Science and Adaptive Analysis*, *17*(01n02), 2550004. https://doi.org/10.1142/S2424922X25500044

[22] Mejbel, B. G., Sarow, S. A., Al-Sharify, M. T., Al-Haddad, L. A., Ogaili, A. A. F., & Al-Sharify, Z. T. (2024). A data fusion analysis and random forest learning for enhanced control and failure diagnosis in rotating machinery. *Journal of Failure Analysis and Prevention*, *24*(6), 2979–2989. https://doi.org/10.1007/s11668-024-02075-6

[23] Sun, W., Zhao, R., Yan, R., Shao, S., & Chen, X. (2017). Convolutional discriminative feature learning for induction motor fault diagnosis. *IEEE Transactions on Industrial Informatics*, *13*(3), 1350–1359. https://doi.org/10.1109/TII.2017.2672988

[24] Kumar, H. S., & Upadhyaya, G. (2023). Fault diagnosis of rolling element bearing using continuous wavelet transform and K-nearest neighbour. *Materials Today: Proceedings*, *92*, 56–60. https://doi.org/10.1016/j.matpr.2023.03.618

[25] Neupane, D., Kim, Y., & Seok, J. (2021). Bearing fault detection using scalogram and switchable normalization-based CNN (SN-CNN). *IEEE Access*, *9*, 88151–88166. https://doi.org/10.1109/ACCESS.2021.3089698

[26] Iranzad, R., & Liu, X. (2025). A review of random forest-based feature selection methods for data science education and applications. *International Journal of Data Science and Analytics*, *20*(2), 197–211. https://doi.org/10.1007/s41060-024-00509-w

[27] Piccialli, V., & Sciandrone, M. (2022). Nonlinear optimization and support vector machines. *Annals of Operations Research*, *314*(1), 15–47. https://doi.org/10.1007/s10479-022-04655-x

[28] Halder, R. K., Uddin, M. N., Uddin, M. A., Aryal, S., & Khraisat, A. (2024). Enhancing K-nearest neighbor algorithm: A comprehensive review and performance analysis of modifications. *Journal of Big Data*, *11*(1), 113. https://doi.org/10.1186/s40537-024-00973-y

[29] Niu, M., Ma, S., Zhu, H., & Xu, K. (2025). Fault diagnosis of rotating machinery using a signal processing technique and lightweight model based on mechanical structural characteristics. *Measurement*, *245*, 116505. https://doi.org/10.1016/j.measurement.2024.116505

[30] Xu, D., & Li, C. (2024). Optimization of deep belief network based on sparrow search algorithm for rolling bearing fault diagnosis. *IEEE Access*, *12*, 10470–10481. https://doi.org/10.1109/ACCESS.2024.3354794

[31] Yang, J., Li, X., & Mao, M. (2025). Fault diagnosis model via vibration signal analysis with an improved BKA-VMD and CNN-TELM hybrid framework. *Energy Science & Engineering*, *13*(2), 781–810. https://doi.org/10.1002/ese3.2036

[32] Tan, C., Yang, L., Chen, H., & Xin, L. (2022). Fault diagnosis method for rolling bearing based on VMD and improved SVM optimized by METLBO. *Journal of Mechanical Science and Technology*, *36*(10), 4979–4991. https://doi.org/10.1007/s12206-022-0911-2

[33] Sanz, J., Perera, R., & Huerta, C. (2012). Gear dynamics monitoring using discrete wavelet transformation and multi-layer perceptron neural networks. *Applied Soft Computing*, *12*(9), 2867–2878. https://doi.org/10.1016/j.asoc.2012.04.003

[34] Hu, P., Zhao, C., Huang, J., & Song, T. (2023). Intelligent and small samples gear fault detection based on wavelet analysis and improved CNN. *Processes*, *11*(10), 2969. https://doi.org/10.3390/pr11102969

[35] Moosavian, A., Ahmadi, H., Tabatabaeefar, A., & Khazaee, M. (2013). Comparison of two classifiers; K-nearest neighbor and artificial neural network, for fault diagnosis on a main engine journal-bearing. *Shock and Vibration*, *20*(2), 263–272. https://doi.org/10.3233/SAV-2012-00742

[36] Wang, Z., Liu, Y., Bai, R., Chen, H., Li, J., Chen, X., . . . , & Chu, F. (2025). Multi-modal multi-scale multi-level fusion quadrant entropy for mechanical fault diagnosis. *Expert Systems with Applications*, *281*, 127715. https://doi.org/10.1016/j.eswa.2025.127715

[37] Wang, Z., Zhang, M., Chen, H., Li, J., Li, G., Zhao, J., . . . , & Chu, F. (2025). A generalized fault diagnosis framework for rotating machinery based on phase entropy. *Reliability Engineering & System Safety*, *256*, 110745. https://doi.org/10.1016/j.ress.2024.110745

[38] Wang, Z., Liang, P., Bai, R., Liu, Y., Zhao, J., Yao, L., . . . , & Chu, F. (2025). Few-shot fault diagnosis for machinery using multi-scale perception multi-level feature fusion image quadrant entropy. *Advanced Engineering Informatics*, *63*, 102972. https://doi.org/10.1016/j.aei.2024.102972

[39] Wang, X., Si, S., Wei, Y., & Li, Y. (2019). The optimized multi-scale permutation entropy and its application in compound fault diagnosis of rotating machinery. *Entropy*, *21*(2), 170. https://doi.org/10.3390/e21020170

[40] Khaniki, M. A. L., Mirzaeibonehkhater, M., & Manthouri, M. (2023). Enhancing fault detection in induction motors using LSTM-attention neural networks. In *2023 9th International Conference on Control, Instrumentation and Automation*, 1–5. https://doi.org/10.1109/ICCIA61416.2023.10506369

[41] Jandaghi, E., Chen, X., & Yuan, C. (2023). Motion dynamics modeling and fault detection of a soft trunk robot. In *2023 IEEE/ASME International Conference on Advanced Intelligent Mechatronics*, 1324–1329. https://doi.org/10.1109/AIM46323.2023.10196206

[42] Irani, H., Ghahremani, Y., Kermani, A., & Metsis, V. (2025). Time series embedding methods for classification tasks: A review. *Expert Systems*, *42*(11), e70148. https://doi.org/10.1111/exsy.70148

[43] Wang, B., Kestelyn, X., Kharazian, E., & Grolet, A. (2024). Application of normal form theory to power systems: A proof of concept of a novel structure-preserving approach. In *2024 IEEE Power & Energy Society General Meeting* (pp. 1–5). https://doi.org/10.1109/PESGM51994.2024.10688514

[44] Atmaja, B. T., Ihsannur, H., Suyanto, & Arifianto, D. (2024). Lab-scale vibration analysis dataset and baseline methods for machinery fault diagnosis with machine learning. *Journal of Vibration Engineering & Technologies*, *12*(2), 1991–2001. https://doi.org/10.1007/s42417-023-00959-9

[45] Liang, W.-K., Tseng, P., Yeh, J.-R., Huang, N. E., & Juan, C.-H. (2021). Frontoparietal beta amplitude modulation and its interareal cross-frequency coupling in visual working memory. *Neuroscience*, *460*, 69–87. https://doi.org/10.1016/j.neuroscience.2021.02.013

[46] Nguyen, V.-T., & Nguyen, M.-T. (2025). Advanced noise reduction for in-cylinder combustion pressure data using ICEEMDAN and optimal wavelet selection. *IEEE Access*, *13*, 62029–62044. https://doi.org/10.1109/ACCESS.2025.3558428

[47] Masuda, M., & Shiiba, T. (2024). Temporal and frequency analysis with empirical mode decomposition for vehicle vibration signals. In *16th International Symposium on Advanced Vehicle Control: Proceedings of AVEC*, 468–473. https://doi.org/10.1007/978-3-031-70392-8_67

[48] Civera, M., & Surace, C. (2021). A comparative analysis of signal decomposition techniques for structural health monitoring on an experimental benchmark. *Sensors*, *21*(5), 1825. https://doi.org/10.3390/s21051825

[49] Bhatti, S., Shaikh, A. A., Mansoor, A., & Hussain, M. (2024). New approaches of stochastic models to examine the vibration features in roller bearings. *Applied Sciences*, *14*(4), 1616. https://doi.org/10.3390/app14041616

[50] Kumar, A., Wang, J., Parkash, C., Sharma, V., & Tang, H. (2025). Development of a robust wavelet divergence-based framework for health monitoring and remaining useful life estimation of gearbox. *Results in Engineering*, *27*, 106373. https://doi.org/10.1016/j.rineng.2025.106373

[51] Shah, K., Patel, H., Sanghvi, D., & Shah, M. (2020). A comparative analysis of logistic regression, random forest and KNN models for the text classification. *Augmented Human Research*, *5*(1), 12. https://doi.org/10.1007/s41133-020-00032-0

[52] Qi, K., & Yang, H. (2022). Elastic net nonparallel hyperplane support vector machine and its geometrical rationality. *IEEE Transactions on Neural Networks and Learning Systems*, *33*(12), 7199–7209. https://doi.org/10.1109/TNNLS.2021.3084404

[53] Costa, V. G., & Pedreira, C. E. (2023). Recent advances in decision trees: An updated survey. *Artificial Intelligence Review*, *56*(5), 4765–4800. https://doi.org/10.1007/s10462-022-10275-5

[54] Stelzer, F., Röhm, A., Vicente, R., Fischer, I., & Yanchuk, S. (2021). Deep neural networks using a single neuron: Folded-in-time architecture using feedback-modulated delay loops. *Nature Communications*, *12*(1), 5164. https://doi.org/10.1038/s41467-021-25427-4

[55] Liu, D., Cui, L., & Wang, H. (2023). Rotating machinery fault diagnosis under time-varying speeds: A review. *IEEE Sensors Journal*, *23*(24), 29969–29990. https://doi.org/10.1109/JSEN.2023.3326112

[56] Bai, Y., Cheng, W., Wen, W., & Liu, Y. (2023). Application of time-frequency analysis in rotating machinery fault diagnosis. *Shock and Vibration*, *2023*(1), 9878228. https://doi.org/10.1155/2023/9878228

[57] Peng, Z. K., Peter, W. T., & Chu, F. L. (2005). A comparison study of improved Hilbert–Huang transform and wavelet transform: Application to fault diagnosis for rolling bearing. *Mechanical Systems and Signal Processing*, *19*(5), 974–988. https://doi.org/10.1016/j.ymssp.2004.01.006

[58] Martinez-Ríos, E. A., Bustamante-Bello, R., Navarro-Tuch, S., & Perez-Meana, H. (2023). Applications of the generalized Morse wavelets: A review. *IEEE Access*, *11*, 667–688. https://doi.org/10.1109/ACCESS.2022.3232729

How to Cite: Nguyen, V.-T., Le, B.-T., & Dao, V.-P. (2026). Enhanced Rotating Machinery Fault Diagnosis Using Holo-Hilbert Spectrum Analysis and Machine Learning. *Journal of Computational and Cognitive Engineering*. https://doi.org/10.47852/bonviewJCCE62027633